IEEE Access
Multidisciplinary | Rapid Review | Open Access Journal

Received 8 August 2023, accepted 18 September 2023, date of publication 26 September 2023, date of current version 27 October 2023.

Digital Object Identifier 10.1109/ACCESS.2023.3319558

SURVEY

A Review of Diagnostic Strategies for Pulmonary Embolism Prediction in Computed Tomography Pulmonary Angiograms

JYOTHI CHILLAPALLI[1], SHILPA GITE[1], (Member, IEEE), BUNNY SAINI[1], KETAN KOTECHA[2], AND SULTAN ALFARHOOD[3]

[1]Department of Computer Science and Engineering, Symbiosis Institute of Technology, Symbiosis International (Deemed University), Pune 412115, India
[2]Symbiosis Centre for Applied Artificial Intelligence, Symbiosis Institute of Technology, Symbiosis International (Deemed University), Pune 412115, India
[3]Department of Computer Science, College of Computer and Information Sciences, King Saud University, Riyadh 11543, Saudi Arabia

Corresponding author: Shilpa Gite (shilpa.gite@sitpune.edu.in)

This work was supported by Symbiosis International (Deemed University), Pune, India.

ABSTRACT Pulmonary Embolism (PE) occurs when blood clots travel to the lungs from different parts of the body. It is amongst the most lethal cardio-respiratory diseases after stroke and heart attack. It occurs due to injury or inactivity due to Deep Vein Thrombosis (DVT). Over the last decade, the PE mortality rate has increased by 23%. Moreover, Vein Thromboembolism has been one of the leading causes of mortality among hospitalized COVID-19 patients. As a result, the necessity for early pulmonary embolism identification has immense significance in saving human lives. Computed Tomography Pulmonary Angiograms (CTPA) are the optimal medical imaging technique for diagnosing pulmonary embolism because of their superior sensitivity and specificity. The ability to distinguish between malignant and benign lungs using CTPA is critical for the early identification of the disease. The field of medical imaging analysis has significantly advanced due to the use of Machine Learning (ML) and Deep Learning (DL) techniques, notably Convolutional Neural Networks (CNN), for automated disease detection. These Computer-Aided Diagnosis (CAD) systems assist healthcare workers in rapid and knowledgeable decision-making, improving patient outcomes globally. This review paper offers a systematic study of current improvements in identifying PE by medical image processing, motivated by an extensive overview. This study attempts to bridge the gap between research and practice by providing a broad framework that covers both baseline and state-of-the-art approaches. It is a valuable resource for researchers and medical practitioners by providing insights into the effective utilization of advanced techniques at each stage of medical image analysis.

INDEX TERMS Pulmonary embolism, CNN, ensemble learning, COVID-19.

I. INTRODUCTION

Pulmonary Embolism (PE) is caused by blood clots that travel from other human body areas to the lungs, blocking a pulmonary artery [1]. It is part of a more significant condition known as Deep Vein Thrombosis (DVT), which causes blood clots in the veins. DVT is a blood clot commonly occurring in the legs, arms, or other veins. Patients who have just had surgery are recommended to stay in bed. Blood clots might form during this time due to damage or inactivity of body parts. These clots break off the vein walls, releasing dimers or fragments [2]. These dimers go through the veins to the lungs, obstructing part or all of the blood supply, resulting in Pulmonary Embolism.

Approximately 50% of DVTs can result in silent PEs. PE and DVT impact nearly 3 to 6 lakh people in the United States annually [3]. Within three months of being diagnosed, 15% to 30% die. DVT has a high mortality rate of up to 25%;

The associate editor coordinating the review of this manuscript and approving it for publication was Chuan Li.

treatment drops to 2 to 11% [4]. According to a necroscopy review, PE is responsible for 5% to 10% of hospitalized patients' fatalities [1]. Among COVID-19 patients hospitalized, venous thromboembolism has been one of the primary reasons for death [5]. PE has become a frequent occurrence in individuals diagnosed with COVID-19, with documented prevalence rates of 16.5% overall and escalating to 24.7% among severe cases admitted to the Intensive Care Unit (ICU) as per reports [109]. COVID-19 patients, particularly those in critical condition requiring ICU admission, exhibit an increased risk of developing PE, affecting up to one-third of cases [110]. CTPA serves as a diagnostic modality for confirming clinical suspicions of PE, including cases related to COVID-19. 43.3% of ICU patients are likely to get diagnosed with DVT [6]. Acute PE can cause a life-threatening condition like pulmonary hypertension and right ventricular dysfunction or failure [7]. As a reaction to PE before cardiac failure, there is typically an increase in breathing and pulse rate. Being one of the arterial system problems, PE is a complex disease to diagnose; early detection and treatment can save lives. It is a preventable cause of death if diagnosed early, although delays in identification and treatment increase the chance of death.

A. PRIOR RESEARCH RELATED TO THIS WORK

There are just a few reviews available to identify pulmonary embolism. Paper [8] is one of the most recent reviews. The authors thoroughly reviewed existing literature that uses deep learning approaches to detect PE in this work. However, [8] focuses solely on retrospective studies with a limited assessment of pooled performance due to heterogeneity across studies, a high risk of bias in certain studies, and the absence of real-world applications. Our research aims to provide a comprehensive analysis of recent advancements in the field, considering the developments beyond the scope of [8]. Additionally, we aim to perform a thorough performance comparison of recent and benchmark studies in this domain. Our review article aims to expand the body of research by addressing the highlighted gaps and expanding the scope of analysis.

Research [4] provides information on pulmonary embolism, pulmonary nodule disorders, pneumonia, and other lung disorders. The current state of deep neural networks in medical imagery is described in this paper. It contains a complete study of the models that produced positive outcomes, laying a crucial research foundation for researchers interested in this field.

The survey [9] looks at recent U-Net architecture trends. It covers a wide range of deep learning developments. It also covers the many imaging modalities and application areas that U-Net has improved. The study [10] examined the whole pipeline of medical imaging and analysis procedures concerned with COVID-19. It focuses on X-ray and CT modalities commonly employed in frontline hospitals. Review [11] demonstrates how using Artificial Intelligence (AI) in the management of COVID-19 infection might assist in optimizing resources and boost efficiency.

Table 1 presents the existing review papers available in this domain.

The research gap identified in these papers is as follows:

- Unsupervised learning methods need to be investigated to reduce the time-consuming task of human label categorization in supervised learning algorithms.
- There must be a significant gap in assessing the clinical impact of automated PE detection on patient care. Studies should focus on examining the usefulness of these systems in a realistic context.
- The lack of labelled data available for training affects the effectiveness of DL models. Other approaches to overcome this include using adversarial models to generate image samples and supplement the current training data.
- Manual labelling of imaging data is costly and time-consuming. Hence, self-supervised and transfer learning systems should be explored.

Limitations of the review papers are as follows:

- None provide theoretical knowledge on various categories in which PE can be classified. The focus is only on the diagnosis of PE and not on classification.
- Most of the PE papers reviewed implemented baseline models for the diagnosis of PE.
- For PE diagnosis, datasets are not extensively reviewed.
- Advanced research directions are not mentioned in the case of PE disease.

The authors intend to overcome these limitations in this review, and the highlights are summarized as follows:

- It includes papers that provide theoretical knowledge regarding the various types of PEs. This knowledge can be used to develop systems focusing on classifying PE.
- It provides a detailed analysis of available datasets.
- It comprises a generalized framework that involves baseline and advanced technologies for each stage of medical image analysis.
- AI-powered algorithms for diagnosing COVID-19 are considered to provide advanced research directions for PE diagnosis and classification.

This paper is organized as follows: Section II reviews the current works available for PE and COVID-19 using CTPA/CT modality. The generalized framework is mentioned in Section III; each stage is discussed in detail. Detailed reviews of all the models are presented in the Performance analysis subsection III-G. Section IV discusses the insights derived from this extensive study. Finally, Conclusions and Future Directions are presented in Section V.

II. EXISTING WORKS

This section is divided into five sections. Section A provides knowledge about PE and possible categories for classifying PE. Section B includes papers that focus on the automatic detection of PE. Artificial Intelligence (AI) techniques used for diagnosing COVID-19 are mentioned in Section C. Papers

TABLE 1. Comparison of review papers.

Reference	Objectives and Topic	Discussion	Limitations	Type
[4]	This paper examines major deep-learning approaches for classifying, detecting, and segmentation of pulmonary medical images.	The review of research articles published between 1962-2019. No. of research articles studied is 181. Detailed analysis of available datasets explored. Detailed analysis of models that achieved produced positive results is explored.	The focus is only on lung diseases. Lack of new trends in the research area since 2019.	Review
[8]	This research thoroughly reviews the literature on PE detection using deep learning algorithms on CTPA.	The focus is on PE detection only on CTPA. Test accuracies were calculated for five studies.	There is no direct comparison between the performance of the deep learning system and that of the radiologist. More advanced research directions need to be explored.	Systematic Review and Meta-Analysis
[9]	This survey explores the U-Net architecture's multiple innovations, breakthroughs, and recent trends.	U-Net-based models have been applied to all imaging modalities. The focus is only on U-Net architectures.	Only four architectures are included for comparison with U-Net.	Review
[10]	For COVID-19, this survey focuses on combining AI methods and X-ray CT modalities.	Focuses on image acquisition, segmentation, diagnosis, and follow-up of COVID-19. Future directions are explored.	Datasets should be extensively reviewed.	Review
[11]	This paper includes AI techniques applied for the detection of COVID-19. It shows how AI applied to thoracic radiology optimizes the workflow of radiologists.	Focuses on CT and X-ray modalities.	Limitations, Challenges, and Future directions should have been included in this work. Datasets are not reviewed.	Review

that enhanced the baseline models using AI algorithms are referred to in Section D. Section E briefs on papers that proposed Deep CNNs and Ensemble learning as diagnostic strategies for PE and COVID-19 diseases.

A. PULMONARY EMBOLISM AND CLASSIFICATION OF PULMONARY EMBOLISM

PE refers to the situation caused by blood clots that travel to the lungs and block the pulmonary arteries. PE can be classified based on clot location (Saddle/ Lobar/ Segmental/ Subsegmental), temporality (Acute/ Chronic) and hemodynamic compromise (Massive/ Submassive/ Low-risk). Massive PE is indicated by pulmonary hypotension or distress; the arterial pressure is less than 90 mm Hg. Submassive PE is hemodynamically stable. The dysfunction in the right ventricle with an end-diastolic diameter greater than one can be taken as a feature to be observed in CTPA. Low Risks PE is acute PE without clinical signs that define massive and submassive PE [1]. The impact of embolism and unsteady flow in acute PE, the diameter of the enlarged pulmonary artery can be noticed. The vessel is distal to the occlusion and is decreased in Chronic PE. CTPA contains a distal wedge flaw with an oblique angle with the vessel wall [12].

B. AUTOMATIC DETECTION OF PULMONARY EMBOLISM

The primary method for PE diagnosis is CTPA, which involves a technician painstakingly tracing each stem of the pulmonary vein for any possible PEs. CTPA assessment is time-taking activity, and its precision is influenced by human errors, such as the ability to focus and sensitivity to PE visual elements. CAD can improve PE diagnosis and reduce the time to read CTPA datasets [13].

For the automatic detection of PE, a two-stage CNN model was developed. Stage one employs a unique 3D fully CNN for a candidate proposal that searches the entire CTPA volume for a set of cubes containing suspected PEs. In stage two, each proposal cube is adjusted to align it with the vessel's position, and the adjusted cubes are sent into a 2D classifier to eliminate false positives. The system's performance on CTPA with tiny PEs in sub-segmental arteries is yet to be investigated [14].

Reference [15] proposed a More Accurate Faster R-CNN (MA Faster R-CNN), which combines a Multi-scale Fusion Feature Pyramid Network (MF-FPN) and Residual Prediction Module (RPM) for the detection of PE. Finetuned SE-ResNet-50 + MF-FPN is also included. The feature map generated by MF-FPN uses an RPN network to generate region proposals which help improve detection accuracy and reliability [15]. Reference [16] proposed a two-stage algorithm. The first stage is a 3D DCNN, a region proposal stage. The second stage is a false positive reduction stage. It uses a loss function called Sample Weighted Categorical Cross-Entropy (SWCCE) to minimize the false positives [16].

Reference [17] introduced Iodine maps from Dual-energy CT angiograms [18], [19]. 11 out of 1144 CTPAs, i.e. 1.0% CTPAs, had a new diagnosis of PE after using iodine maps [17]. A pre-trained AlexNet with appropriate finetuning CNN and an AlexNet built from scratch detected PE automatically. The findings revealed that a finetuned pre-trained CNN surpassed a CNN trained anew and that CNNs that were finetuning were more robust to variations in training set size. Based on the amount of data provided, the layer-wise finetuning scheme offered can assist in achieving optimal performance [13].

C. AI TECHNIQUES USED FOR AUTOMATIC DETECTION OF COVID-19

Intelligent platforms for COVID-19 imaging are mentioned in [10]. Segmentation, Diagnosis, and Prognosis using Machine Learning (ML) techniques are discussed. U-Net, UNet++, V-Net, VB-Net. ResNet-50, CNN, and RF-based classification models were reviewed for diagnosis of COVID-19. According to the research, ML-based technique and multidisciplinary integration could motivate COVID-19 experiments to be followed [10].

D. AI TECHNIQUES WERE USED TO ENHANCE THE BASELINE MODELS

A previous study proposed a network architecture incorporating a feature-wise attention layer and CNNs [21]. The results demonstrated the superior performance of the suggested feature-wise attention layer compared to the stacked attention architecture. COVID-SegNet is a deep neural network model designed for segmenting COVID-19 infection regions from chest CT scans. It contains the Feature Variation (FV) block and Progressive Atrous Spatial Pyramid Pooling (PASPP). The network showed increased COVID-19 pneumonia segmentation performance, resolving the difficulty of recognizing COVID-19 pneumonia [22].

In a separate work, [23] proposed the UNet++ model, enhancing segmentation quality. Mask R-CNN++ is an enhanced version that combines Mask R-CNN with UNet++ for effective instance segmentation [23]. The architecture [24] comprises two main modules; the first module includes the data augmentation phase, which uses classical data augmentation methods and Conditional Generative Adversarial Nets (CGAN), and the second module is the Deep Transfer Learning (DTL) model. Different data augmentation methods, such as rotation, shifting, flipping, etc., were applied to the original dataset. CGANs involve generator and discriminator networks, which helps in subduing the overfitting problem caused by the limited data. Cascaded SE-ResUNet is a primary segmentation network based on the structure of U-Net. A residual network induces finer gradient movement to provide better feature representation, while squeeze-and-excitation (SE) blocks are used as an attention mechanism [25].

Fuse-TSD is an algorithm for distinguishing healthy from deadly lung nodules. The three types of features calculated are the GLCM and Fourier shape descriptors, and the last was obtained from an eight-layer DCNN. BPNN [26], [27] and AdaBoost [28], [29] based ensemble classifiers were developed for each feature type. The three classifiers' decisions are combined using a weighted sum of probability. The algorithm effectively differentiated between normal and malignant lumps [30].

E. CNNs AND ENSEMBLE LEARNING

Reference [31] has built a model with ensemble learners by fusing eight deep CNN learners. Networks like AlexNet, GoogleNet, ResNet, etc., are fused by majority voting (VOT), averaging (AVE), or machine learning algorithms. SVM, MLP, GBRT, and RF achieved the most satisfactory results. VOT and AVE yield higher recall than the ML algorithms [31]. A stacked ensemble model was developed considering the following pre-trained models: VGG-19, ResNet-101, and DenseNet-169. A metric was devised to choose three base classifiers. The stacked ensemble achieved higher recall and accuracy than the baseline and existing models [32].

As mentioned above, a major part of the study is focused on the automatic identification of PE, and the findings have been promising. In all methods proposed in the literature, the specificity and sensitivity attained are greater than 75%. The limitations: lack of dataset in a paper focusing on COVID-19, system not being efficient enough to detect PE in subsegmental arteries, artefacts, and fractures, causing false predictions. More importantly, it is observed that there are very few papers on the classification of PE. Various segmentation and diagnosis techniques were designed for COVID-19 detection. AI techniques, Deep CNNs, and Ensemble Learning were used to enhance the performance of those models. So, these models can be used to design a standard model for classifying PE.

III. THE GENERALIZED FRAMEWORK

Figure 1 depicts a generalized framework consisting of six stages: Data Collection, Data Processing, Data Augmentation, Data Segmentation, Feature Extraction, CNN Classifiers, and Performance Analysis. In this section, each of these stages is discussed in detail.

A. DATA COLLECTION

Table 2 lists the available datasets that provide CTPAs to research PE disease.

1) RSNA-STR Pulmonary Embolism CT (RSPECT) Dataset - To increase the use of ML in PE diagnostics, the RSNA® has partnered with the STR. In the training set, there are 7279 studies. The images are organized into study and series directories. They are in Digital Imaging and Communications in Medicine (DICOM) format and include additional metadata [34]. Figure 2 shows an example of a DICOM image.
2) FUMPE Dataset - FUMPE is a public dataset that contains CT angiograms for PE of 35 different subjects. Using a semi-automated image-processing software tool, two radiologist professionals contributed the ground truth for each benchmark image [35].
3) CAD-PE Dataset - 91 computed tomography pulmonary angiograms positive for pulmonary embolism in this dataset. At least one experienced radiologist has segmented all clots in each image. The dataset was created for the CAD-PE ISBI challenge [33].
4) CTPA Pulmonary Embolism - The dataset utilized in [15] was created by expert radiologists at the

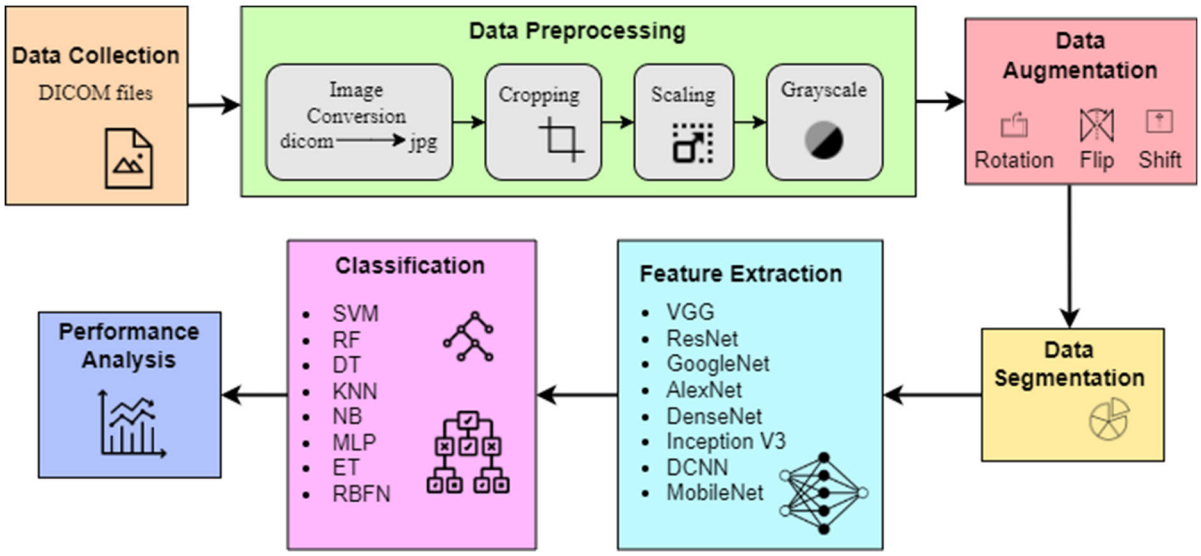

FIGURE 1. The generalized framework for PE classification.

TABLE 2. Datasets available for PE diagnosis using CTPAs.

Reference	Dataset Name	Application and Purpose	Created By	Subject	Sample	Dataset Link
[15]	CTPA Pulmonary Embolism	This data was utilized for training and testing a pulmonary embolism detection algorithm.	China-Japan Friendship Hospital	30 patients	7771 CTPA	
[33]	CAD-PE	This dataset was created for research in computer-aided detection of pulmonary embolism.	Serrano G. G.		91 CTPA	https://ieee-dataport.org/open-access/cad-pe
[14]	PE129	This dataset was created to evaluate an algorithm used for PE detection.	Yang et al.		129 CTPA	
[34]	RSNA-STR Pulmonary Embolism CT (RSPECT)	This dataset can be used for predicting the existence and characteristics of PE.	Radiological Society of North America (RSNA®) Society of Thoracic Radiology (STR)		1.94m CTPA	https://www.kaggle.com/c/rsna-str-pulmonary-embolism-detection/data
[35]	Ferdowsi University of Mashhad's PE (FUMPE)	This dataset was generated to research computer-aided pulmonary embolism detection.	Masoudi et al.	35 patients	8792 CTPA	https://www.kaggle.com/andrewmvd/pulmonary-embolism-in-ct-images
[36]	CTPA Data	This dataset was used to propose an algorithm that can identify CTPAs with APE.	Liu et al.		590 CTPA	
[16]	CTPA Dataset	This dataset was used to propose an algorithm for PE detection.	Weikert et al.		1465 CTPA	

China-Japan Friendship Hospital and is unavailable to the public. A sequence of DICOM format images in the collection represents each patient. For this study, 7771 CTPA slice images with pulmonary embolism were chosen. The training dataset contains 3736 images, the validation dataset 1737 images, and the testing dataset 2298 images [15].

5) PE129 Dataset - The PE129 CTPA dataset was randomly divided into a training set of 100 scans and a test set of 29 scans [14].

6) CTPA Dataset - CTPAs (n=1465) conducted at the University of Basel, Petersgraben, are included in this dataset [16]. These CTPAs were manually labelled as positive (n = 232) or negative (n = 1233). The location of the embolus was also determined (central, segmental, peripheral).

CTPA Data - [36] includes APE and non-APE patients. A total of 590 cases were gathered retrospectively. 460 patients with APE and 130 patients without APE took part. The dataset was randomly split into a training dataset

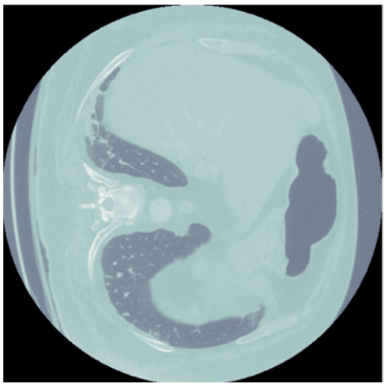

FIGURE 2. DICOM image.

(80%) and a tuning dataset (20%) to obtain effective segmentation results.

B. DATA PREPROCESSING

Data preprocessing on CT scans [37] is done by completing the below steps:

1) Image Conversion - The retrieved datasets are in Dicom format. The conversion is done to improve the clarity and cleanliness of the images. Aside from that, the Dicom image's information can be eliminated, leaving only the objects visible.
2) Cropping - The next step is to crop the data. Cropping is used to draw attention to the current CT image lung item by leaving a dark background.
3) Scaling - Because the cropping procedure produces varying image dimensions, scaling is utilized to uniformize the image dimensions.
4) Grayscale - Grayscale ensures that the image's grayscale is consistent. Because the radiography image value will only have pixel values ranging from 0-255, a grayscale technique will be employed in the image scaling process, with black as 0 (lowest) and white as 1 (highest) [38].

C. DATA AUGMENTATION

CNNs require a vast volume of data to be trained, so small datasets demand data augmentation techniques [21], [39]. Data augmentation aims to generate more data of similar patterns to increase the number of training images [20], [38], [40], [41]. The following are the types of data augmentations techniques:

1) Spatial Augmentation: Mirroring, Elastic Deformations, Rotations, Scaling, Flip (Horizontal and Vertical), Shift (Horizontal and Vertical), Zoom [42].
2) Color Augmentation: Brightness, Contrast, Gamma alterations [42].
3) Noise Augmentation: Adding Gaussian noise [38].

The Mixup Data Augmentation approach enhanced the networks' generalization capability. Compared to traditional methods, the experimental results shown in the study [21] proved that the mixup methodology performed better. CGAN and classical data augmentation approaches helped generate more images and resolve the overfitting problem caused by the limited data [24], [43].

D. DATA SEGMENTATION

In image processing and analysis, segmentation is a crucial stage. It delineates the regions of interest (ROIs) in the chest CT images [10]. Recent literature on nodule segmentation reports better nodule segmentation using deep learning [44], [45], [46], [47]. This subsection summarizes a list of segmentation works as well as their applications.

C-SE-ResUNet is a classic encoder-decoder model. Convolution blocks and max-pooling procedures are utilized in its encoder to retrieve important semantic data. Fine-grained data is obtained from Skip connections. The decoder merges this data for precise localization and segmentation [25]. COVID-SegNet [22] combines FV and PASPP to improve feature representation and address COVID-19 infection's challenging shape variations. The designed network improved segmentation capabilities while also delivering excellent performance results.

U-Net is a technique for segmenting images [48], [49], [50]. In this network, skip connections are utilized to connect downsampling and upsampling layers, allowing downsampling layers to transfer features straight to upsampling layers. This method enables the U-net to assess the image's entire context, resulting in an end-to-end segmentation map [51]. Many studies have applied the U-net structure for medical image segmentation and created enhancements based on it [4], [52], [53], [54].

Reference [9] reviews U-Net and its variants for medical image segmentation. UNet++ [23], [55], [56], [57] is a neural design for semantic and instance segmentation. It is an ensemble of U-Nets of different depth that partly shares an encoder and co-learn. It redesigns skip connections at the decoder sub-networks to combine features of differing semantic scales and devises a pruning scheme to achieve significant speedup. The neural network architecture and hyperparameters account for the most crucial constituent of a medical image segmentation procedure.

Reference [20] employed a typical 3D U-Net model with no specific modifications to reduce extraneous parameters. The authors constructed an exact and efficient segmentation model using k-fold cross-validation on 20 CT scans of COVID-19 without overfitting on a small dataset. The 3D U-Net framework [58], [59], [60], [61] extends the standard U-Net architecture to allow 3D volumetric segmentation. With only a few annotated samples, this network can segment images. 3D samples have many recurring patterns and forms, allowing for quicker training, although sparsely annotated data [9].

The residual blocks are used as the fundamental convolutional block in V-Net [62], [63], [64]. During the training process, the network optimization is performed using the Dice coefficient, which enables the network to handle

imbalanced situations where the foreground and background voxels differ significantly in number [65]. The segmentation network called VB-Net [66], [67], [68], based on deep learning, was specifically developed to automatically segment and quantify COVID-19-infected regions in CT scans. The automatic infection region delineation was found to have a high degree of accuracy in a quantitative evaluation [68].

E. FEATURE EXTRACTION

This subsection is divided into features, Feature Extraction Techniques, and Deep Learning Techniques for feature extraction.

1) FEATURES

One of the most significant steps is feature extraction, which incorporates techniques and algorithms for identifying replica forms. The Segmentation output is used to extract features [69]. Features that were taken into consideration during extracting features are Correlation, Contrast, Homogeneity, SD (Standard Deviation), Root Mean Square (RMS), Variance, Skewness, Kurtosis, IDM (Image Difference Measure), Dissimilarity, ASM (Angular Secondary Moment), etc. Although these features are not new, they can provide new insights into the progression of classification in PE [70].

2) FEATURE EXTRACTION TECHNIQUES

Table 3 mentions the list of features and feature extraction techniques. GLCM is a method for extracting features [71], [72], [73]. It is used to extract the images' second-degree statistical information. It comprises the relationships between distinct angles in an image's pixels [74], [75]. This approach was applied in [30] to distinguish the heterogeneity of lung nodule voxel values. Calculated the energy, contrast, entropy, and inverse difference to measure the spatial dependence of voxel values, which proved beneficial for image classification. At 0°, 45°, 90°, and 135°, four GLCMs were recorded for each image patch; it yielded a 16-D GLCM texture descriptor [30]. Reference [70] used GLCM for images of segmented lung regions. Contrast, Correlation, Energy, and Homogeneity were the features used [70], [75]. Other GLCM-extracted features [76] are listed in Table 3. Kirsch compass kernels are used in the LDP method to integrate the directional elements. The LDP approach generates an output matrix with the exact dimensions as the input image. For classifier input, this matrix is turned into a vector. GLRLM extracts high-level texture characteristics [72], [73], [76]. It generates a feature vector that can be used to input a classifier. The GLSZM algorithm [73] is an upgraded version of the GLRLM algorithm. Small/Long zone emphasis, grey-level variation, size zone variance, and so on are all extracted [74], [76]. To describe the heterogeneity of the nodule structure, [30] computed the Fourier descriptor. The computation included locating the gravity centre on the input, graphing the length between the point and the gravity centre against the length traversed by this point along the nodule boundary, and then applying the Fourier transform. 52 low-frequency coefficients were selected as the Fourier descriptors [30]. The SURF algorithm is implemented in [69]. It is a fast and reliable approach for representing and comparing images in a local, similarity-invariant manner. The SURF technique's fundamental attraction is its potential to swiftly compute operators using box filters and enabling real-time applications [77]. DWT [74], [78], [79] divides the image into frequency subbands and uses an h low-pass and a g high-pass filter to extract the features listed in Table 3.

TABLE 3. Feature extraction techniques and the list of features extracted.

Feature Extraction Techniques	Features extracted
Grey Level Co-occurrence Matrix (GLCM)	ASM, Contrast, Correlation, Variance, IDM, Average, Entropy, Autocorrelation, Dissimilarity, Cluster Shade, Cluster Prominence, Max. Probability, Energy, Homogeneity
Local Directional Pattern (LDP)	Texture, Contrast, Variance
Grey Level Run Length Matrix (GLRLM)	Short/Long run emphasis, non-uniformity, Run percentage, low grey/high grey level run emphasis.
Grey Level Size Zone Matrix (GLSZM)	Small/Long zone emphasis, non-uniformity, zone percentage, low grey/high grey level zone emphasis, Small/Large zone low grey level emphasis, Small/Large zone high grey-level emphasis, grey-level variance, size zone variance
Fourier Shape Descriptor (FSD)	Heterogeneity, Low-frequency coefficients
Speeded Up Robust Features (SURF)	RMS, Variance, Smoothing, Skewness, Kurtosis, IDM, Contrast, Correlation, Energy, Homogeneity, Mean, Standard Deviation, Entropy
Discrete Wavelet Transform (DWT)	Low-frequency, horizontal high-frequency, high vertical frequency

3) DEEP LEARNING TECHNIQUES FOR FEATURE EXTRACTION

a) AlexNet: - Five Convolutional Layers (CL) with three pooling, a softmax layer, and two fully connected layers are included in this network. The first layer inputs a $227 \times 227 \times 3$ image and comprises 96 $11 \times 11 \times 3$ kernels. Overlapping max-pooling layers follow the two CL layers. The Rectified Linear Unit (ReLu) is used as the activation function [80], [81]. The study [82], 1000 characteristics are extracted from the final layer.

b) ResNet – Various versions are determined by the number of layers, such as ResNet 18, 50, and 101. It learns from the residual features during training [83], [84], [85]. Reference [82] employed the ResNet-50 architecture to generate 1000 features.

c) VGG19 - It's a visual geometry group's 19-layer deep CNN, similar to AlexNet. VGG19 consists of 16 convolutional layers, three entirely connected, five MaxPool layers, and one SoftMax layer, with input dimensions $224 \times 224 \times 3$ [21, s, t]. Reference [82] collected 1000 features from the last layer.

d) DenseNet - DenseNets are organized into dense blocks, with the number of filters varying but the feature map

size remaining constant inside each block [81], [82]. References [32], In a work, [85] used DenseNet-169 with 169 layers as a part of their model architecture.

e) Inception V3 – It is a deep CNN with 48 layers. The model uses parallelized operations, quantized convolutions, and dimension reduction to guarantee efficiency [82], [83], [85].

f) Eight-layer D-CNN - Three convolutional layers were used in this DCNN model, each with 32, 32, and 64 kernels of size 5×5. A 2-stride 3×3 average-pooling layer follows each convolutional layer. The final two layers are fully connected. Convolutional and fully connected layers use ReLU to perform a nonlinear conversion from input to output [30].

g) MobileNet - It is a CNN for mobile vision applications because of its lightweight architecture, including only 30 layers. MobileNet employs depth-wise separable convolution, which indicates it performs convolution on each colour channel separately instead of merging and flattening them. As a result, MobileNet training is more efficient [84], [85], [86].

F. CLASSIFICATION

This subsection includes Machine Learning classifiers implemented by the reviewed papers. A summary of the classification techniques used is provided in Table 4.

TABLE 4. Classification techniques used in the reviewed papers.

Reference	Classification Techniques Utilized in the Paper							
	MLP	KNN	SVM	NB	RF	DT	RBFN	ET
[46]	Yes	Yes	Yes					
[47]	Yes	Yes	Yes	Yes	Yes			
[35]			Yes					
[34]	Yes	Yes		Yes	Yes	Yes	Yes	
[45]			Yes		Yes			Yes

1) Naïve Bayes (NB) classifier - This rule-based predictive model assumes substantial interdependence between features when provided a target class. The resulting model is simple to fit and performs excellently [87], [88], [89].

2) Multilayer Perceptron (MLP) classifier - A feed-forward neural network is what the multilayer perceptron is called. A multilayer perceptron's architecture varies, but typically, it comprises multiple layers of interconnected neurons. Each node in a multilayer perceptron is interconnected with every other node in the preceding and succeeding layers [79], [89], [90].

3) Radial Basis Function Network (RBFN) classifier - An RBF network [91] is a feed-forward neural network containing the input layer, the hidden layer, and the output layer. As an activation function, it employs radial basis functions [89], [92].

4) K Nearest Neighbor (KNN) classifier - KNN classifier is an instance-based model that uses a distance function to relate unknown groups. It determines a class based on its neighbours. Identifying the neighbours and deciding which class they belong to are the two stages of a KNN classification [89], [93], [94].

5) Random Forest (RF) classifier - RF trains with numerous decision trees and outputs the most frequent class. It constructs a classification tree using randomly selected features at each node [88], [95], [96].

6) Decision Table (DT) Classifier - DT resembles a hierarchical table. Every entry from a higher level is fragmented in this table, which is created using the values of two extra features [96], [97].

7) Extra Trees (ET) Classifier - ET [98] is a machine learning technique widely used to address classification and regression problems as part of an ensemble. The different tree classifier creates many unpruned DTs from the training dataset. To produce predictions, the majority voting technique is employed. Each decision tree casts a vote, and the prediction with the most votes is regarded as the final classification result.

8) Support Vector Machine (SVM) Classifier - The general concept of SVM is to use a nonlinear approach to create a high-dimensional space from feature vectors and then employ linear classifiers. The second method is to use a high-margin hyperplane to separate the data. This is the optimum plane for separating data to the greatest extent possible [88], [89], [94], [98], [99], [100].

G. PERFORMANCE ANALYSIS

This subsection comprises three subsubsections dedicated to the discussion of deployed metrics for performance analysis of several models, along with their comprehensive comparison.

1) Quantitative Analysis Metrics

The total of positive samples identified as positive, negative samples identified as positive, negative samples identified as negative, and the total of positive samples identified as negative are all symbolized by True Positive (TP), False Positive (FP), True Negative (TN), and False Negative (FN), respectively. Table 5 presents the confusion matrix.

TABLE 5. Confusion matrix.

Actual Labels	Predicted Labels	
	Positive	Negative
Positive	TP	FN
Negative	FP	TN

To evaluate the classification techniques, we use the five widely used instances, which are:

a) Accuracy: The accuracy metric calculates the ratio of correctly predicted samples to total samples.

$$Accuracy = \left(\frac{TP + TN}{TP + TN + FP + FN}\right) \quad (1)$$

b) Precision: The precision metric quantifies the ratio of correctly predicted positive samples to all the positive predictions.

$$Precision = (TP) \big/ (TP + FP) \quad (2)$$

c) Recall/Sensitivity: The sensitivity metric accurately assesses the correct identification of positive samples among all the positive samples.

$$Recall/Sensitivity = (TP) \big/ (TP + FN) \quad (3)$$

d) Specificity: The metric specificity measures rightly predicted negative samples against all negative ones.

$$Specificity = (TN) \big/ (TN + FP) \quad (4)$$

e) F1-Score: The F1 Score measures the overall performance. It is the harmonic mean of precision and recall.

$$F1 - Score = 2 \times \left(\frac{Precision \times Recall}{Precision + Recall}\right) \quad (5)$$

2) Performance Comparison of recent works on deep learning techniques for pulmonary embolism detection using CTPAs

Reference [14] developed a two-stage CNN model for automatic PE diagnosis. The first stage uses a 3D FCN for a candidate proposal that extracts 3D feature hierarchies from the CTPA volume to create a set of suspected PE cubes. The second stage involves transforming each proposal cube to orient it with the affected vessel's direction. Three cross-sections of the modified candidate cube are retrieved for false-positive elimination to generate a three-channel input to the ResNet-18-based 2D classification network. The numerous small emboli in the PE129 dataset were the reason for more significant improvements. The authors extensively tested this system on the available datasets to improve the performance [14].

Reference [16] created a cloud-based PE detection prototype system for a two-stage R-CNN. The first stage uses 3D DCNN, which comprises a ResNet architecture trained on segmented scans and generates a 3D segmentation map. Region proposals are generated from the segmentation map and input into the algorithm's second stage. The second stage is a false positive reduction stage. It uses SWCCE, a loss function, to minimize the false positives. The loss function is crucial in machine learning because it defines how precisely an algorithm works on particular data. Contrast agents, pulmonary veins, and lymph nodes caused the bulk of false-positive observations. This approach offered excellent diagnostic performance for PE [16].

MA Faster R-CNN [15] is a pulmonary embolism detection method. It is composed of MF-FPN and RPM. The Finetuned SE-ResNet-50 + MF-FPN has been added to improve the network's feature extraction capability. It could correct many neglected detections and even detect the smaller emboli accurately. Mapping the primary feature layer of the neighbouring output layer to the output layer achieved stability between semantic and location data. RPM improved the accuracy of classification. The developed model has a greater identification accuracy than the original Faster R-CNN and effectively overcomes the wrong and skipped detection of PE.

Reference [101] developed the PE-Net, a 3-D convolutional model for diagnosing PE on CT scans. It is a realistic model that accepts volumetric CTPA exams without time-consuming and computationally intensive preparation and shows long-term performance. The model can automatically generate an explainable prediction value, allowing for unbiased analysis of PE positive risk and the development of appropriate limits for medical applications in detection procedures.

Reference [36] used multiple probability thresholds to assess U-Net's performance for clot identification, and sensitivity, specificity, and area under the curve (AUC) were chosen as evaluation measures. They also examined the relationship between the clot burden derived from this model. It exhibits a high AUC for detecting pulmonary emboli and can quantify the clot burden in Acute Pulmonary Embolism (APE) patients.

A performance Comparison of recent works on deep learning techniques for pulmonary embolism detection using CTPAs is presented in Table 6.

3) Performance comparison of advanced techniques used for diagnosis of COVID-19 using CTs

Table 7 provides the performance comparison of advanced techniques used to diagnose COVID-19 using CTs.

A hybrid method is proposed in [102]. The image is segmented into discrete high/low-frequency Intrinsic Mode Functions (IMFs) using two-dimensional Empirical Mode Decomposition (2DEMD) after the raw CT-scan image is transformed into a single grayscale image. Next, the decomposition residue is eliminated, and all the IMFs are combined to create a refined CT-scan image. This enhancement gives the image more scope for visual analysis and extracts the image's frequency texture profiles. The modified image is then trained using VGG16 and VGG19. Regarding accuracy and F1 score, models trained using modified CT-scan images outperformed models trained with raw images. This work provides a new perspective for researchers to employ 2DEMD's feature extraction power as a performance-enhancing criterion for CT-scan image classification [102].

A prior work [21] introduced a specialized network that leverages a feature-wise attention layer to enhance the

TABLE 6. Performance comparison of recent works on deep learning techniques for pulmonary embolism detection using CTPAs.

Reference	Year	Modality	Methods	Results
[14]	2019	CT	FCN ResNet-18	Sensitivity: 76.3%
[16]	2020	CT	3D DCNN ResNet	Specificity: 95.5% PPV: 79.6% NPV: 98.6% F1 Score: 0.86
[15]	2021	CT	MA Faster R-CNN	AP: 85.88% Sensitivity: 87.30% Specificity: 86.29%
[101]	2020	CT	PENet	Accuracy: 80% AUROC: 0.85 Specificity: 81% Sensitivity: 75% PPV: 44% NPV: 94% AUC: 0.93
[36]	2021	CT	UNet	Sensitivity: 94.6% Specificity: 76.5%
[103]	2022	CT	InceptionResnet V2 + LSTM (Pre-training: Chest X-rays)	Sensitivity: 86.6% Specificity: 93.5% ROC AUC score: 0.94
			InceptionResnet V2 + LSTM (Pre-training: Natural Img)	Sensitivity: 83.5% Specificity: 90.7% ROC AUC score: 0.91
[104]	2022	CT	3D CNN Sequential Model with Attention Gradient-Weighted Class Activation Mapping	AUROC: 0.93 Sensitivity: 0.86 Specificity: 0.85
[105]	2022	CT	2D segmentation model: UNet + Xception encoder (Scan level)	Sensitivity: 0.80 Specificity: 0.74 Accuracy: 0.76 AUC: 0.85
[106]	2023	CT	Hybrid 3D/2D UNet topology	Sensitivity: 91.4% Specificity: 91.5% Accuracy: 91.5%
[107]	2023	CT	Pytorch UNet	Sensitivity: 0.95 Precision: 0.93 F1 Score: 0.94 AUC: 0.88
[108]	2023	CT	Anatomically aware dual-hop learning	Sensitivity: 0.929 Specificity: 0.961 PPV: 0.891 NPV: 0.975 F1: 0.910

* AUROC= Area Under the Receiver Operating Characteristics, PPV= Positive Predictive Value, NPV= Negative Predictive Value

representation of features obtained by CNNs. Furthermore, the mixup data augmentation method has increased the network's initial performance. The proposed attention-based models (ResNet50, ResNet101, ResNext50 32 × 4d, DenseNet201, VGG19) are compared to stacking attention networks (AttentionNet-56, AttentionNet-92), as well as traditional versus mixup data augmentation methodologies in this research. While outperforming the stacked attention variations, feature-wise attention extension and mixup data augmentation yield significant improvements over the baseline CNN. The ResNet50 model, which integrated a feature-wise attention layer and was trained on mixup augmented data, achieved an accuracy of 95.57% and exhibited the best performance [21].

COVID-SegNet [22] was developed for segmenting COVID-19 infection areas and the entire lung from chest CT scans. An FV block is suggested to resolve the underlying issue in identifying COVID-19-affected zones, hence alleviating the difficulty in differentiating COVID-19 pneumonia from the lungs. It improves contrast and changes the strength of the features in a variety of images automatically and adaptively. It obtains the global parameter by using channel attention to generate new features. By pooling these features, feature representation for COVID-19 segmentation can be considerably improved. As a result, the network uses PASPP, which combines data from atrous convolutional layers over time, effectively combining input from several scales. COVID-19 pneumonia segmentation performance is improved by obtaining more useful contextual features.

Cascaded SE-ResUNet is proposed in the study [25]. The system is cascaded because it uses six SE-ResUNet networks: a wide segmentation network to detect ROIs and a good

TABLE 7. Performance comparison of advanced techniques used for diagnosis of COVID-19 using CTs.

Reference	Models	Performance Results				
		Accuracy	F1-Score	Precision	Sensitivity	Specificity
[102]	VGG16 (Modified CT scans using 2DEMD)	84.06	84.68	81.5	-	80
	VGG19 (Modified CT scans using 2DEMD)	85.63	85.16	82.5	-	83.53
[21]	ResNet50 + Attention Layer +Mixup Data augmentation	95.57	95.61	-	-	-
[22]	COVID-SegNet (UNet4 + FV + PASPP)	-	-	99	98.6	-
[25]	C-SE-ResUNet (Multi organ segmentation)	-	97.01(Lung-L) 96.63(Lung-R)	-	-	-
[32]	VGG19 + DenseNet-169 + ResNet-101 (COVID-CT Dataset)	84.73	85.71	78.15	-	-
	VGG19 + DenseNet-169 + ResNet-101 (COVID-CTset)	99	99	99	-	-
	VGG19 + DenseNet-169 + ResNet-101 (SARS-CoV-2 CT-scan dataset)	93.5	93.78	89.91	-	-
[74]	GLCM + SVM (10-fold)	98.91	98.81	99.1	98.52	99.23
	LDP +SVM (2-fold)	50.94	45.05	46.74	43.72	57.09
	GLRLM + SVM (10-fold)	96.41	96.2	93.75	98.78	94.38
	GLSZM + SVM (10-fold)	98.77	98.65	99.6	97.72	99.67
	DWT + SVM (10-fold)	97.81	97.6	98.49	96.8	98.66
[24]	AlexNet (Augmentation+ CGAN)	75.73	-	-	63.83	87.62
	VGGNet16 (Augmentation + CGAN)	78.05	-	-	62.77	93.33
	VGGNet19 (Augmentation + CGAN)	73.74	-	-	71.28	76.19
	GoogleNet (Augmentation + CGAN)	77.07	-	-	71.28	82.86
	ResNet50 (Augmentation + CGAN)	81.38	-	-	80.85	81.9

segmentation network to get enhanced segmentation accuracy organically. Dice Loss (F1 score) and an adjustive CT window are utilized to improve the robustness of the segmentation of small organs. The StructSeg 2019 Challenge awarded this framework first prize [25].

In the case of COVID-19, lowering the number of FNs is critical for controlling the virus's transmission. To detect COVID-19, [32] presented a stacked ensemble model with pre-trained and fully connected layers. A systematic approach and a diversity metric were used to create the stacked ensemble of VGG-19, DenseNet169, and ResNet-101 models. Generation, selection, and aggregation were the three stages of the systematic approach. During the generation phase, pre-trained models were employed to construct a pool of basic classifiers containing models with varied topologies. During the selection step, the stacked ensemble's base classifiers were picked from a group of base classifiers. The diversity and accuracy measurements are often used to identify the ensemble's base classifiers. The weighted average of base classifiers' outputs is fed into the meta-classifier during aggregation. The stacked ensemble model beat the baseline and current models on three chest CT scan datasets, obtaining good accuracy and recall [32].

The classification of coronaviruses in the paper [74] is done in two steps. The classification method was applied to four different subsets during the first step. SVM was used to classify the subgroups once they were transformed into vectors. In the second stage, features were extracted using five distinct methods, including GLCM, LDP, GLRLM, GLSZM, and DWT, and then classified using SVM. Cross-validation methods of 2-fold, 5-fold, and 10-fold were applied during the classification procedure. During 10-fold cross-validation, the classification accuracy of the GLCM, GLSZM, and DWT techniques was always greater than 90%.

IV. DISCUSSION

In this review paper, we have thoroughly examined the body of research on automatic PE detection. Our study offers

insights and practical ramifications by carefully analyzing various research papers.

- Significantly, CNNs have shown encouraging outcomes, highlighting their potential to increase diagnostic accuracy in the field.
- In recent research, there has been a notable inclination towards utilizing the U-Net architecture for diagnosing PE.
- Additionally, multitask or multistage strategies are also being adopted in the diagnostic process. These methods involve extracting relevant features or masks from medical scans and proceeding to the image segmentation phase. This process aims to enhance the overall functionality of the models.
- Creating a sizable enough annotated training set is time-consuming and expensive, and smaller datasets can lead to overfitting. This highlights the need for more studies to examine self-supervised or unsupervised approaches.
- Although CAD systems have made huge advances in PE detection, their incorporation into clinical practice still needs to be improved. Studies often need to pay more attention to the clinical implications of their work, needing thorough research.

For COVID-19 identification in chest CT scan pictures, classic data augmentation approaches are combined with CGAN based on a DTL model. Limited COVID-19 chest CT scans are classified using DTL models. In combination with CGAN, the traditional data augmentations produced more images and helped overcome the overfitting problem. This study used five deep CNN-based models to detect Coronavirus-infected patients using chest CT radiographs (AlexNet, VGGNet16, VGGNet19, GoogleNet, and ResNet50). The end-to-end structure of DTL models eliminates the need for standard feature extraction and selection methods. In all deep transfer models tested, traditional data augmentations combined with CGAN improve classification performance [24].

All the models mentioned in Table 7 provide great results except for the model which included LDP and SVM, along with 2-fold cross-validation.

V. CONCLUSION AND FUTURE RECOMMENDATIONS

Computer-aided diagnostics can effectively solve the pulmonary Embolism problem. This work presents and discusses a review of recent pulmonary embolism-related work using AI techniques. Many studies focused on automatic PE detection using CTPAs, and the results have been promising. In all methods mentioned in the literature, the specificity and sensitivity attained are greater than 75%. It has been noted that there are very few articles on the classification of PE based on clot location and hemodynamic compromise. So, to provide a novel method for PE classification, the authors have reviewed various segmentation and diagnosis techniques used for COVID-19 disease. The shortcomings include a need for more training data in the research focusing on COVID-19 and the system's incorrect predictions caused by artefacts and fractures. Various AI approaches were included to improve the models' performance. So, these models can be finetuned to design a standard model for the classification of PE. Though several AI-based ongoing kinds of research exist to solve this problem, PE would be an interesting domain.

Future work in this area could concentrate on resolving one of the following research gaps observed in the PE-related papers:

1) Classification strategy- Models which can classify CTPAs into all possible categories still need to be developed.
2) Analysis of factors-The potential relationship between clot burden and patient risk categorization still needs to be analyzed.
3) Accurate clinical models- More studies on reducing the FN rate are needed. Models' performance in a prospective clinical setting has yet to be determined.
4) Technical Advancements- Performance of advanced technologies for diagnosing and classifying PE is yet to be explored.
5) Improvement in CNN-based models-To achieve proper convergence, training a deep CNN network is problematic since it requires a considerable quantity of annotated training samples and a high skill level. Using a large set of labelled images to finetune a CNN is a viable alternative. So, we intend to finetune models used for COVID-19 diagnosis and develop a standardized model specific to PE.

All these are identified future research directions, and their solutions would assist the clinicians in focusing on specific types of PE and developing a treatment plan for each. This will aid in the early detection and treatment of PE patients, lowering their fatality rate worldwide and will help humanity in the long run.

REFERENCES

[1] E.-O. Essien, P. Rali, and S. C. Mathai, "Pulmonary embolism," *Med. Clinics North Amer.*, vol. 103, no. 3, pp. 549–564, May 2019, doi: 10.1016/j.mcna.2018.12.013.

[2] S. C. Park, B. E. Chapman, and B. Zheng, "A multistage approach to improve performance of computer-aided detection of pulmonary embolisms depicted on CT images: Preliminary investigation," *IEEE Trans. Biomed. Eng.*, vol. 58, no. 6, pp. 1519–1527, Jun. 2011, doi: 10.1109/TBME.2010.2063702.

[3] *The Surgeon General's Call to Action to Prevent Deep Vein Thrombosis and Pulmonary Embolism*, Office Surgeon General (US); Section I: Deep Vein Thrombosis Pulmonary Embolism Major Public Health Problems, Office Surgeon Gen. (US); Nat. Heart, Lung, Blood Inst. (US), Rockville, MD, USA, 2008. [Online]. Available: https://www.ncbi.nlm.nih.gov/books/NBK44181/

[4] J. Ma, Y. Song, X. Tian, Y. Hua, R. Zhang, and J. Wu, "Survey on deep learning for pulmonary medical imaging," *Frontiers Med.*, vol. 14, no. 4, pp. 450–469, Aug. 2020, doi: 10.1007/s11684-019-0726-4.

[5] C. P. Marini, E. Lewis, P. Petrone, A. Zenilman, Z. Lu, A. Rivera, and J. McNelis, "Incidence and effects of deep vein thrombosis on the outcome of patients with coronavirus disease 2019 infection," *J. Vascular Surg., Venous Lymphatic Disorders*, vol. 10, no. 4, pp. 803–810, Jul. 2022, doi: 10.1016/j.jvsv.2021.10.013.

[6] Y. Fares, Y. C. Sinzogan-Eyoum, P. Billoir, A. Bogaert, G. Armengol, K. Alexandre, J. Lammens, M. Grall, H. Levesque, Y. Benhamou, and S. Miranda, "Systematic screening for a proximal DVT in COVID-19 hospitalized patients: Results of a comparative study," *J. Médecine Vasculaire*, vol. 46, no. 4, pp. 163–170, Jul. 2021, doi: 10.1016/j.jdmv.2021.05.003.

[7] N. Chaosuwannakit, W. Soontrapa, P. Makarawate, and K. Sawanyawisuth, "Importance of computed tomography pulmonary angiography for predict 30-day mortality in acute pulmonary embolism patients," *Eur. J. Radiol. Open*, vol. 8, Jan. 2021, Art. no. 100340, doi: 10.1016/j.ejro.2021.100340.

[8] S. Soffer, E. Klang, O. Shimon, Y. Barash, N. Cahan, H. Greenspana, and E. Konen, "Deep learning for pulmonary embolism detection on computed tomography pulmonary angiogram: A systematic review and meta-analysis," *Sci. Rep.*, vol. 11, no. 1, p. 15814, Aug. 2021, doi: 10.1038/s41598-021-95249-3.

[9] N. Siddique, S. Paheding, C. P. Elkin, and V. Devabhaktuni, "U-net and its variants for medical image segmentation: A review of theory and applications," *IEEE Access*, vol. 9, pp. 82031–82057, 2021, doi: 10.1109/ACCESS.2021.3086020.

[10] F. Shi, J. Wang, J. Shi, Z. Wu, Q. Wang, Z. Tang, K. He, Y. Shi, and D. Shen, "Review of artificial intelligence techniques in imaging data acquisition, segmentation, and diagnosis for COVID-19," *IEEE Rev. Biomed. Eng.*, vol. 14, pp. 4–15, 2021, doi: 10.1109/RBME.2020.2987975.

[11] M. D. C. Abelaira, F. C. Abelaira, A. Ruano-Ravina, and A. Fernández-Villar, "Use of conventional chest imaging and artificial intelligence in COVID-19 Infection. A review of the literature," *Open Respiratory Arch.*, vol. 3, no. 1, Jan. 2021, Art. no. 100078, doi: 10.1016/j.opresp.2020.100078.

[12] G. Kim and H. Natcheva, "Imaging of cardiovascular thoracic emergencies," *Radiologic Clinics North Amer.*, vol. 57, no. 4, pp. 787–794, Jul. 2019, doi: 10.1016/j.rcl.2019.02.012.

[13] N. Tajbakhsh, J. Y. Shin, S. R. Gurudu, R. T. Hurst, C. B. Kendall, M. B. Gotway, and J. Liang, "Convolutional neural networks for medical image analysis: Full training or fine tuning?" *IEEE Trans. Med. Imag.*, vol. 35, no. 5, pp. 1299–1312, May 2016, doi: 10.1109/TMI.2016.2535302.

[14] X. Yang, Y. Lin, J. Su, X. Wang, X. Li, J. Lin, and K.-T. Cheng, "A two-stage convolutional neural network for pulmonary embolism detection from CTPA images," *IEEE Access*, vol. 7, pp. 84849–84857, 2019, doi: 10.1109/ACCESS.2019.2925210.

[15] H. Yuan, Y. Shao, Z. Liu, and H. Wang, "An improved faster R-CNN for pulmonary embolism detection from CTPA images," *IEEE Access*, vol. 9, pp. 105382–105392, 2021, doi: 10.1109/ACCESS.2021.3099479.

[16] L. Schmuelling, F. C. Franzeck, C. H. Nickel, G. Mansella, R. Bingisser, N. Schmidt, B. Stieltjes, J. Bremerich, A. W. Sauter, T. Weikert, and G. Sommer, "Deep learning-based automated detection of pulmonary embolism on CT pulmonary angiograms: No significant effects on report communication times and patient turnaround in the emergency department nine months after technical implementation," *Eur. J. Radiol.*, vol. 141, Aug. 2021, Art. no. 109816, doi: 10.1016/j.ejrad.2021.109816.

[17] E. K. Weidman, A. J. Plodkowski, D. F. Halpenny, S. A. Hayes, R. Perez-Johnston, J. Zheng, C. Moskowitz, and M. S. Ginsberg, "Dual-energy CT angiography for detection of pulmonary emboli: Incremental benefit of iodine maps," *Radiology*, vol. 289, no. 2, pp. 546–553, Nov. 2018, doi: 10.1148/radiol.2018180594.

[18] L. Yu, A. N. Primak, X. Liu, and C. H. McCollough, "Image quality optimization and evaluation of linearly mixed images in dual-source, dual-energy CT: Dual-source, dual-energy CT linearly mixed images," *Med. Phys.*, vol. 36, no. 3, pp. 1019–1024, Feb. 2009, doi: 10.1118/1.3077921.

[19] J. C. G. Sánchez, M. Magnusson, M. Sandborg, Å. C. Tedgren, and A. Malusek, "Segmentation of bones in medical dual-energy computed tomography volumes using the 3D U-Net," *Phys. Medica*, vol. 69, pp. 241–247, Jan. 2020, doi: 10.1016/j.ejmp.2019.12.014.

[20] D. Müller, I. Soto-Rey, and F. Kramer, "Robust chest CT image segmentation of COVID-19 lung infection based on limited data," *Informat. Med. Unlocked*, vol. 25, Jan. 2021, Art. no. 100681, doi: 10.1016/j.imu.2021.100681.

[21] Ö. Özdemir and E. B. Sönmez, "Attention mechanism and mixup data augmentation for classification of COVID-19 computed tomography images," *J. King Saud Univ.-Comput. Inf. Sci.*, vol. 34, no. 8, pp. 6199–6207, Sep. 2022, doi: 10.1016/j.jksuci.2021.07.005.

[22] Q. Yan, B. Wang, D. Gong, C. Luo, W. Zhao, J. Shen, J. Ai, Q. Shi, Y. Zhang, S. Jin, L. Zhang, and Z. You, "COVID-19 chest CT image segmentation network by multi-scale fusion and enhancement operations," *IEEE Trans. Big Data*, vol. 7, no. 1, pp. 13–24, Mar. 2021, doi: 10.1109/TBDATA.2021.3056564.

[23] Z. Zhou, M. M. R. Siddiquee, N. Tajbakhsh, and J. Liang, "UNet++: Redesigning skip connections to exploit multiscale features in image segmentation," *IEEE Trans. Med. Imag.*, vol. 39, no. 6, pp. 1856–1867, Jun. 2020, doi: 10.1109/TMI.2019.2959609.

[24] M. Loey, G. Manogaran, and N. E. M. Khalifa, "A deep transfer learning model with classical data augmentation and CGAN to detect COVID-19 from chest CT radiography digital images," *Neural Comput. Appl.*, vol. 1, pp. 1–13, Oct. 2020, doi: 10.1007/s00521-020-05437-x.

[25] Z. Cao, B. Yu, B. Lei, H. Ying, X. Zhang, D. Z. Chen, and J. Wu, "Cascaded SE-ResUnet for segmentation of thoracic organs at risk," *Neurocomputing*, vol. 453, pp. 357–368, Sep. 2021, doi: 10.1016/j.neucom.2020.08.086.

[26] S. Bauer, R. Wiest, L.-P. Nolte, and M. Reyes, "A survey of MRI-based medical image analysis for brain tumor studies," *Phys. Med. Biol.*, vol. 58, no. 13, pp. R97–R129, Jul. 2013, doi: 10.1088/0031-9155/58/13/R97.

[27] M. Lather and P. Singh, "Investigating brain tumor segmentation and detection techniques," *Proc. Comput. Sci.*, vol. 167, pp. 121–130, Jan. 2020, doi: 10.1016/j.procs.2020.03.189.

[28] J. Feulner, S. Kevin Zhou, M. Hammon, J. Hornegger, and D. Comaniciu, "Lymph node detection and segmentation in chest CT data using discriminative learning and a spatial prior," *Med. Image Anal.*, vol. 17, no. 2, pp. 254–270, Feb. 2013, doi: 10.1016/j.media.2012.11.001.

[29] D. Yifan, L. Jialin, and F. Boxi, "Forecast model of breast cancer diagnosis based on RF-AdaBoost," in *Proc. Int. Conf. Commun., Inf. Syst. Comput. Eng. (CISCE)*, Beijing, China, May 2021, pp. 716–719, doi: 10.1109/CISCE52179.2021.9445847.

[30] Y. Xie, J. Zhang, Y. Xia, M. Fulham, and Y. Zhang, "Fusing texture, shape and deep model-learned information at decision level for automated classification of lung nodules on chest CT," *Inf. Fusion*, vol. 42, pp. 102–110, Jul. 2018, doi: 10.1016/j.inffus.2017.10.005.

[31] E. Jangam and C. S. R. Annavarapu, "A stacked ensemble for the detection of COVID-19 with high recall and accuracy," *Comput. Biol. Med.*, vol. 135, Aug. 2021, Art. no. 104608, doi: 10.1016/j.compbiomed.2021.104608.

[32] B. Zhang, S. Qi, P. Monkam, C. Li, F. Yang, Y.-D. Yao, and W. Qian, "Ensemble learners of multiple deep CNNs for pulmonary nodules classification using CT images," *IEEE Access*, vol. 7, pp. 110358–110371, 2019, doi: 10.1109/ACCESS.2019.2933670.

[33] G. G. Serrano, "CAD-PE," IEEE DataPort, Oct. 17, 2019, doi: 10.21227/9BW7-6823.

[34] E. Colak et al., "The RSNA pulmonary embolism CT dataset," *Radiol., Artif. Intell.*, vol. 3, no. 2, Mar. 2021, Art. no. e200254, doi: 10.1148/ryai.2021200254.

[35] M. Masoudi, H.-R. Pourreza, M. Saadatmand-Tarzjan, N. Eftekhari, F. S. Zargar, and M. P. Rad, "A new dataset of computed-tomography angiography images for computer-aided detection of pulmonary embolism," *Sci. Data*, vol. 5, no. 1, Sep. 2018, Art. no. 180180, doi: 10.1038/sdata.2018.180.

[36] W. Liu, M. Liu, X. Guo, P. Zhang, L. Zhang, R. Zhang, H. Kang, Z. Zhai, X. Tao, J. Wan, and S. Xie, "Evaluation of acute pulmonary embolism and clot burden on CTPA with deep learning," *Eur. Radiol.*, vol. 30, no. 6, pp. 3567–3575, Jun. 2020, doi: 10.1007/s00330-020-06699-8.

[37] T. Badriyah, N. Sakinah, I. Syarif, and D. R. Syarif, "Machine learning algorithm for stroke disease classification," in *Proc. Int. Conf. Electr., Commun., Comput. Eng. (ICECCE)*, Istanbul, Turkey, Jun. 2020, pp. 1–5, doi: 10.1109/ICECCE49384.2020.9179307.

[38] A. R. Beeravolu, S. Azam, M. Jonkman, B. Shanmugam, K. Kannoorpatti, and A. Anwar, "Preprocessing of breast cancer images to create datasets for deep-CNN," *IEEE Access*, vol. 9, pp. 33438–33463, 2021, doi: 10.1109/ACCESS.2021.3058773.

[39] S. Nabavi, A. Ejmalian, M. E. Moghaddam, A. A. Abin, A. F. Frangi, M. Mohammadi, and H. S. Rad, "Medical imaging and computational image analysis in COVID-19 diagnosis: A review," *Comput. Biol. Med.*, vol. 135, Aug. 2021, Art. no. 104605, doi: 10.1016/j.compbiomed.2021.104605.

[40] K. Chaitanya, N. Karani, C. F. Baumgartner, E. Erdil, A. Becker, O. Donati, and E. Konukoglu, "Semi-supervised task-driven data augmentation for medical image segmentation," *Med. Image Anal.*, vol. 68, Feb. 2021, Art. no. 101934, doi: 10.1016/j.media.2020.101934.

[41] C. Chen, K. Zhou, M. Zha, X. Qu, X. Guo, H. Chen, Z. Wang, and R. Xiao, "An effective deep neural network for lung lesions segmentation from COVID-19 CT images," *IEEE Trans. Ind. Informat.*, vol. 17, no. 9, pp. 6528–6538, Sep. 2021, doi: 10.1109/TII.2021.3059023.

[42] D. I. Morís, J. J. de Moura Ramos, J. N. Buján, and M. O. Hortas, "Data augmentation approaches using cycle-consistent adversarial networks for improving COVID-19 screening in portable chest X-ray images," *Expert Syst. Appl.*, vol. 185, Dec. 2021, Art. no. 115681, doi: 10.1016/j.eswa.2021.115681.

[43] S. Motamed, P. Rogalla, and F. Khalvati, "Data augmentation using generative adversarial networks (GANs) for GAN-based detection of pneumonia and COVID-19 in chest X-ray images," *Informat. Med. Unlocked*, vol. 27, Jan. 2021, Art. no. 100779, doi: 10.1016/j.imu.2021.100779.

[44] S. Ather, T. Kadir, and F. Gleeson, "Artificial intelligence and radiomics in pulmonary nodule management: Current status and future applications," *Clin. Radiol.*, vol. 75, no. 1, pp. 13–19, Jan. 2020, doi: 10.1016/j.crad.2019.04.017.

[45] S. Rakesh and S. Mahesh, "Nodule segmentation of lung CT image for medical applications," *Global Transitions Proc.*, vol. 2, no. 1, pp. 80–83, Jun. 2021, doi: 10.1016/j.gltp.2021.01.011.

[46] J. Chen, H. You, and K. Li, "A review of thyroid gland segmentation and thyroid nodule segmentation methods for medical ultrasound images," *Comput. Methods Programs Biomed.*, vol. 185, Mar. 2020, Art. no. 105329, doi: 10.1016/j.cmpb.2020.105329.

[47] X. Liu, L. Yang, J. Chen, S. Yu, and K. Li, "Region-to-boundary deep learning model with multi-scale feature fusion for medical image segmentation," *Biomed. Signal Process. Control*, vol. 71, Jan. 2022, Art. no. 103165, doi: 10.1016/j.bspc.2021.103165.

[48] H. Zhao and N. Sun, "Improved U-Net model for nerve segmentation," in *Image and Graphics* (Lecture Notes in Computer Science), vol. 10667, Y. Zhao, X. Kong, and D. Taubman, Eds. Cham, Switzerland: Springer, 2017, pp. 496–504, doi: 10.1007/978-3-319-71589-6_43.

[49] Z. Huang, Y. Fang, H. Huang, X. Xu, J. Wang, and X. Lai, "Automatic retinal vessel segmentation based on an improved U-Net approach," *Sci. Program.*, vol. 2021, pp. 1–15, Apr. 2021, doi: 10.1155/2021/5520407.

[50] J. Owler, B. Irving, G. Ridgeway, M. Wojciechowska, J. McGonigle, and S. M. Brady, "Comparison of multi-atlas segmentation and U-Net approaches for automated 3D liver delineation in MRI," in *Medical Image Understanding and Analysis* (Communications in Computer and Information Science), vol. 1065, Y. Zheng, B. M. Williams, and K. Chen, Eds. Cham, Switzerland: Springer, 2020, pp. 478–488, doi: 10.1007/978-3-030-39343-4_41.

[51] O. Ronneberger, P. Fischer, and T. Brox, "U-Net: Convolutional networks for biomedical image segmentation," in *Medical Image Computing and Computer-Assisted Intervention—MICCAI 2015* (Lecture Notes in Computer Science), vol. 9351, N. Navab, J. Hornegger, W. M. Wells, and A. F. Frangi, Eds. Cham, Switzerland: Springer, 2015, pp. 234–241, doi: 10.1007/978-3-319-24574-4_28.

[52] Y. Liu, N. Qi, Q. Zhu, and W. Li, "CR-U-Net: Cascaded U-Net with residual mapping for liver segmentation in CT images," in *Proc. IEEE Vis. Commun. Image Process. (VCIP)*, Sydney, NSW, Australia, Dec. 2019, pp. 1–4, doi: 10.1109/VCIP47243.2019.8966072.

[53] M. Baldeon-Calisto and S. K. Lai-Yuen, "AdaResU-Net: Multiobjective adaptive convolutional neural network for medical image segmentation," *Neurocomputing*, vol. 392, pp. 325–340, Jun. 2020, doi: 10.1016/j.neucom.2019.01.110.

[54] N. Ibtehaz and M. S. Rahman, "MultiResUNet: Rethinking the U-Net architecture for multimodal biomedical image segmentation," *Neural Netw.*, vol. 121, pp. 74–87, Jan. 2020, doi: 10.1016/j.neunet.2019.08.025.

[55] Z. Zhou, M. M. R. Siddiquee, N. Tajbakhsh, and J. Liang, "UNet++: A nested U-Net architecture for medical image segmentation," in *Deep Learning in Medical Image Analysis and Multimodal Learning for Clinical Decision Support* (Lecture Notes in Computer Science), vol. 11045, D. Stoyanov, Z. Taylor, G. Carneiro, T. Syeda-Mahmood, A. Martel, L. Maier-Hein, J. M. R. S. Tavares, A. Bradley, J. P. Papa, V. Belagiannis, J. C. Nascimento, Z. Lu, S. Conjeti, M. Moradi, H. Greenspan, and A. Madabhushi, Eds. Cham, Switzerland: Springer, 2018, pp. 3–11, doi: 10.1007/978-3-030-00889-5_1.

[56] S. Wu, Z. Wang, C. Liu, C. Zhu, S. Wu, and K. Xiao, "Automatical segmentation of pelvic organs after hysterectomy by using dilated convolution U-Net++," in *Proc. IEEE 19th Int. Conf. Softw. Qual., Rel. Secur. Companion (QRS-C)*, Sofia, Bulgaria, Jul. 2019, pp. 362–367, doi: 10.1109/QRS-C.2019.00074.

[57] H. Cui, X. Liu, and N. Huang, "Pulmonary vessel segmentation based on orthogonal fused U-Net++ of chest CT images," in *Medical Image Computing and Computer Assisted Intervention—MICCAI 2019* (Lecture Notes in Computer Science), vol. 11769, D. Shen, T. Liu, T. M. Peters, L. H. Staib, C. Essert, S. Zhou, P.-T. Yap, and A. Khan, Eds. Cham, Switzerland: Springer, 2019, pp. 293–300, doi: 10.1007/978-3-030-32226-7_33.

[58] Ö. Çiçek, A. Abdulkadir, S. S. Lienkamp, T. Brox, and O. Ronneberger, "3D U-Net: Learning dense volumetric segmentation from sparse annotation," in *Medical Image Computing and Computer-Assisted Intervention—MICCAI 2016* (Lecture Notes in Computer Science), vol. 9901, S. Ourselin, L. Joskowicz, M. R. Sabuncu, G. Unal, and W. Wells, Eds. Cham, Switzerland: Springer, 2016, pp. 424–432, doi: 10.1007/978-3-319-46723-8_49.

[59] J. Long, E. Shelhamer, and T. Darrell, "Fully convolutional networks for semantic segmentation," in *Proc. IEEE Conf. Comput. Vis. Pattern Recognit. (CVPR)*, Boston, MA, USA, Jun. 2015, pp. 3431–3440, doi: 10.1109/CVPR.2015.7298965.

[60] C. Zhao, J. Han, Y. Jia, and F. Gou, "Lung nodule detection via 3D U-Net and contextual convolutional neural network," in *Proc. Int. Conf. Netw. Netw. Appl. (NaNA)*, Xi'an, China, Oct. 2018, pp. 356–361, doi: 10.1109/NANA.2018.8648753.

[61] Q. Tong, M. Ning, W. Si, X. Liao, and J. Qin, "3D deeply-supervised U-Net based whole heart segmentation," in *Statistical Atlases and Computational Models of the Heart. ACDC and MMWHS Challenges* (Lecture Notes in Computer Science), vol. 10663, M. Pop, M. Sermesant, P.-M. Jodoin, A. Lalande, X. Zhuang, G. Yang, A. Young, and O. Bernard, Eds. Cham, Switzerland: Springer, 2018, pp. 224–232, doi: 10.1007/978-3-319-75541-0_24.

[62] G. R. Pinheiro, R. Voltoline, M. Bento, and L. Rittner, "V-Net and U-Net for ischemic stroke lesion segmentation in a small dataset of perfusion data," in *Brainlesion: Glioma, Multiple Sclerosis, Stroke and Traumatic Brain Injuries* (Lecture Notes in Computer Science), vol. 11383, A. Crimi, S. Bakas, H. Kuijf, F. Keyvan, M. Reyes, and T. Van Walsum, Eds. Cham, Switzerland: Springer, 2019, pp. 301–309, doi: 10.1007/978-3-030-11723-8_30.

[63] Y. Fang, H. Huang, W. Yang, X. Xu, W. Jiang, and X. Lai, "Nonlocal convolutional block attention module VNet for gliomas automatic segmentation," *Int. J. Imag. Syst. Technol.*, vol. 32, no. 2, pp. 528–543, Mar. 2022, doi: 10.1002/ima.22639.

[64] A. Kanakatte, D. Bhatia, and A. Ghose, "Heart region segmentation using dense VNet from multimodality images," in *Proc. 43rd Annu. Int. Conf. IEEE Eng. Med. Biol. Soc. (EMBC)*, Mexico, Nov. 2021, pp. 3255–3258, doi: 10.1109/EMBC46164.2021.9630303.

[65] F. Milletari, N. Navab, and S.-A. Ahmadi, "V-Net: Fully convolutional neural networks for volumetric medical image segmentation," in *Proc. 4th Int. Conf. 3D Vis. (3DV)*, Stanford, CA, USA, Oct. 2016, pp. 565–571, doi: 10.1109/3DV.2016.79.

[66] B. Wang et al., "AI-assisted CT imaging analysis for COVID-19 screening: Building and deploying a medical AI system," *Appl. Soft Comput.*, vol. 98, Jan. 2021, Art. no. 106897, doi: 10.1016/j.asoc.2020.106897.

[67] G. Mu, Z. Lin, M. Han, G. Yao, and Y. Gao, "Segmentation of kidney tumor by multi-resolution VB-nets," in *Kidney Tumor Segmentation Challenge: KiTS19*. Minneapolis, MN, USA: University of Minnesota Libraries Publishing, 2019, doi: 10.24926/548719.003.

[68] F. Shan, Y. Gao, J. Wang, W. Shi, N. Shi, M. Han, Z. Xue, D. Shen, and Y. Shi, "Abnormal lung quantification in chest CT images of COVID-19 patients with deep learning and its application to severity prediction," *Med. Phys.*, vol. 48, no. 4, pp. 1633–1645, Apr. 2021, doi: 10.1002/mp.14609.

[69] K. Roy, S. S. Chaudhury, M. Burman, A. Ganguly, C. Dutta, S. Banik, and R. Banik, "A comparative study of lung cancer detection using supervised neural network," in *Proc. Int. Conf. Opto-Electron. Appl. Opt. (Optronix)*, Kolkata, India, Mar. 2019, pp. 1–5, doi: 10.1109/OPTRONIX.2019.8862326.

[70] J. T. C. Ming, O. M. Rijal, R. M. Kassim, A. Yunus, and N. M. Noor, "Texture-based classification for reticular pattern and ground glass opacity in high resolution computed tomography thorax images," in *Proc. IEEE EMBS Conf. Biomed. Eng. Sci. (IECBES)*, Malaysia, Dec. 2016, pp. 230–234, doi: 10.1109/IECBES.2016.7843448.

[71] W. M. Shaban, A. H. Rabie, A. I. Saleh, and M. A. Abo-Elsoud, "A new COVID-19 patients detection strategy (CPDS) based on hybrid feature selection and enhanced KNN classifier," *Knowl.-Based Syst.*, vol. 205, Oct. 2020, Art. no. 106270, doi: 10.1016/j.knosys.2020.106270.

[72] C. L. Chowdhary and D. P. Acharjya, "Segmentation and feature extraction in medical imaging: A systematic review," *Proc. Comput. Sci.*, vol. 167, pp. 26–36, Jan. 2020, doi: 10.1016/j.procs.2020.03.179.
[73] J. H. Wang, K. A. Wahid, L. V. van Dijk, K. Farahani, R. F. Thompson, and C. D. Fuller, "Radiomic biomarkers of tumor immune biology and immunotherapy response," *Clin. Transl. Radiat. Oncol.*, vol. 28, pp. 97–115, May 2021, doi: 10.1016/j.ctro.2021.03.006.
[74] M. Barstugan, U. Ozkaya, and S. Ozturk, "Coronavirus (COVID-19) classification using CT images by machine learning methods," 2020, *arXiv:2003.09424*, doi: 10.48550/ARXIV.2003.09424.
[75] X. Ou, W. Pan, and P. Xiao, "In vivo skin capacitive imaging analysis by using grey level co-occurrence matrix (GLCM)," *Int. J. Pharmaceutics*, vol. 460, nos. 1–2, pp. 28–32, Jan. 2014, doi: 10.1016/j.ijpharm.2013.10.024.
[76] E. Oyallon and J. Rabin, "An analysis of the SURF method," *Image Process. Line*, vol. 5, pp. 176–218, Jul. 2015, doi: 10.5201/ipol.2015.69.
[77] H. Koyuncu and M. Barstuğan, "COVID-19 discrimination framework for X-ray images by considering radiomics, selective information, feature ranking, and a novel hybrid classifier," *Signal Process., Image Commun.*, vol. 97, Sep. 2021, Art. no. 116359, doi: 10.1016/j.image.2021.116359.
[78] A. Shafique, J. Ahmed, M. U. Rehman, and M. M. Hazzazi, "Noise-resistant image encryption scheme for medical images in the chaos and wavelet domain," *IEEE Access*, vol. 9, pp. 59108–59130, 2021, doi: 10.1109/ACCESS.2021.3071535.
[79] S. Ghosh, S. Das, and R. Mallipeddi, "A deep learning framework integrating the spectral and spatial features for image-assisted medical diagnostics," *IEEE Access*, vol. 9, pp. 163686–163696, 2021, doi: 10.1109/ACCESS.2021.3133338.
[80] M. Muzammil, I. Ali, I. U. Haq, A. A. Khaliq, and S. Abdullah, "Pulmonary nodule classification using feature and ensemble learning-based fusion techniques," *IEEE Access*, vol. 9, pp. 113415–113427, 2021, doi: 10.1109/ACCESS.2021.3102707.
[81] Q. Li, Y. Yang, Y. Guo, W. Li, Y. Liu, H. Liu, and Y. Kang, "Performance evaluation of deep learning classification network for image features," *IEEE Access*, vol. 9, pp. 9318–9333, 2021, doi: 10.1109/ACCESS.2020.3048956.
[82] S. Pathan, P. C. Siddalingaswamy, P. Kumar, M. M. M. Pai, T. Ali, and U. R. Acharya, "Novel ensemble of optimized CNN and dynamic selection techniques for accurate COVID-19 screening using chest CT images," *Comput. Biol. Med.*, vol. 137, Oct. 2021, Art. no. 104835, doi: 10.1016/j.compbiomed.2021.104835.
[83] A. S. M. Shafi, M. B. Rahman, T. Anwar, R. S. Halder, and H. M. E. Kays, "Classification of brain tumors and auto-immune disease using ensemble learning," *Informat. Med. Unlocked*, vol. 24, Jan. 2021, Art. no. 100608, doi: 10.1016/j.imu.2021.100608.
[84] A. Pal, Z. Xue, B. Befano, A. C. Rodriguez, L. R. Long, M. Schiffman, and S. Antani, "Deep metric learning for cervical image classification," *IEEE Access*, vol. 9, pp. 53266–53275, 2021, doi: 10.1109/ACCESS.2021.3069346.
[85] E. F. Ohata, G. M. Bezerra, J. V. S. D. Chagas, A. V. L. Neto, A. B. Albuquerque, V. H. C. D. Albuquerque, and P. P. R. Filho, "Automatic detection of COVID-19 infection using chest X-ray images through transfer learning," *IEEE/CAA J. Autom. Sinica*, vol. 8, no. 1, pp. 239–248, Jan. 2021, doi: 10.1109/JAS.2020.1003393.
[86] A. Halder and B. Datta, "COVID-19 detection from lung CT-scan images using transfer learning approach," *Mach. Learn., Sci. Technol.*, vol. 2, no. 4, Dec. 2021, Art. no. 045013, doi: 10.1088/2632-2153/abf22c.
[87] K. P. Murphy, "Naive Bayes classifiers," Univ. of British Columbia, New York, NY, USA, Tech. Rep. 1, 2006.
[88] L. H. S. Vogado, R. M. S. Veras, F. H. D. Araujo, R. R. V. Silva, and K. R. T. Aires, "Leukemia diagnosis in blood slides using transfer learning in CNNs and SVM for classification," *Eng. Appl. Artif. Intell.*, vol. 72, pp. 415–422, Jun. 2018, doi: 10.1016/j.engappai.2018.04.024.
[89] A. A. Farid, G. I. Selim, and H. A. A. Khater, "A novel approach of CT images feature analysis and prediction to screen for corona virus disease (COVID-19)," *Int. J. Sci. Eng. Res.*, vol. 11, no. 3, pp. 1141–1149, Mar. 2020, doi: 10.14299/ijser.2020.03.02.
[90] M. W. Gardner and S. R. Dorling, "Artificial neural networks (the multilayer perceptron)—A review of applications in the atmospheric sciences," *Atmos. Environ.*, vol. 32, nos. 14–15, pp. 2627–2636, Aug. 1998, doi: 10.1016/S1352-2310(97)00447-0.
[91] J. A. Leonard and M. A. Kramer, "Radial basis function networks for classifying process faults," *IEEE Control Syst.*, vol. 11, no. 3, pp. 31–38, Apr. 1991, doi: 10.1109/37.75576.
[92] S. N. Qasem and S. M. Shamsuddin, "Radial basis function network based on time variant multi-objective particle swarm optimization for medical diseases diagnosis," *Appl. Soft Comput.*, vol. 11, no. 1, pp. 1427–1438, Jan. 2011, doi: 10.1016/j.asoc.2010.04.014.
[93] P. Cunningham and S. J. Delany, "K-nearest neighbour classifiers—A tutorial," *ACM Comput. Surveys*, vol. 54, no. 6, pp. 1–25, Jul. 2022, doi: 10.1145/3459665.
[94] J. Mukherjee, M. Kar, A. Chakrabarti, and S. Das, "A soft-computing based approach towards automatic detection of pulmonary nodule," *Biocybernetics Biomed. Eng.*, vol. 40, no. 3, pp. 1036–1051, Jul. 2020, doi: 10.1016/j.bbe.2020.03.006.
[95] G. Chassagnon et al., "AI-driven quantification, staging and outcome prediction of COVID-19 pneumonia," *Med. Image Anal.*, vol. 67, Jan. 2021, Art. no. 101860, doi: 10.1016/j.media.2020.101860.
[96] M. Pal, "Random forest classifier for remote sensing classification," *Int. J. Remote Sens.*, vol. 26, no. 1, pp. 217–222, Jan. 2005, doi: 10.1080/01431160412331269698.
[97] R. Kohavi, "The power of decision tables," in *Machine Learning: ECML-95* (Lecture Notes in Computer Science), vol. 912, N. Lavrac and S. Wrobel, Eds. Berlin, Germany: Springer, 1995, pp. 174–189, doi: 10.1007/3-540-59286-5_57.
[98] S. M. M. Hasan, M. F. Rabbi, A. I. Champa, and M. A. Zaman, "A comparative study of classification approaches for COVID-19 prediction," in *Proc. Int. Conf. Inf. Commun. Technol. Sustain. Develop. (ICICT4SD)*, Dhaka, Bangladesh, Feb. 2021, pp. 105–109, doi: 10.1109/ICICT4SD50815.2021.9396890.
[99] F. V. Farahani, A. Ahmadi, and M. H. F. Zarandi, "Hybrid intelligent approach for diagnosis of the lung nodule from CT images using spatial kernelized fuzzy c-means and ensemble learning," *Math. Comput. Simul.*, vol. 149, pp. 48–68, Jul. 2018, doi: 10.1016/j.matcom.2018.02.001.
[100] R. V. M. D. Nobrega, S. A. Peixoto, S. P. P. da Silva, and P. P. R. Filho, "Lung nodule classification via deep transfer learning in CT lung images," in *Proc. IEEE 31st Int. Symp. Computer-Based Med. Syst. (CBMS)*, Karlstad, Sweden, Jun. 2018, pp. 244–249, doi: 10.1109/CBMS.2018.00050.
[101] S.-C. Huang, T. Kothari, I. Banerjee, C. Chute, R. L. Ball, N. Borus, A. Huang, B. N. Patel, P. Rajpurkar, J. Irvin, J. Dunnmon, J. Bledsoe, K. Shpanskaya, A. Dhaliwal, R. Zamanian, A. Y. Ng, and M. P. Lungren, "PENet—A scalable deep-learning model for automated diagnosis of pulmonary embolism using volumetric CT imaging," *npj Digit. Med.*, vol. 3, no. 1, p. 61, Apr. 2020, doi: 10.1038/s41746-020-0266-y.
[102] N. I. Hasan, "A hybrid method of COVID-19 patient detection from modified CT-scan/chest-X-ray images combining deep convolutional neural network and two-dimensional empirical mode decomposition," *Comput. Methods Programs Biomed. Update*, vol. 1, Jan. 2021, Art. no. 100022, doi: 10.1016/j.cmpbup.2021.100022.
[103] H. Huhtanen, M. Nyman, T. Mohsen, A. Virkki, A. Karlsson, and J. Hirvonen, "Automated detection of pulmonary embolism from CT-angiograms using deep learning," *BMC Med. Imag.*, vol. 22, no. 1, p. 43, Dec. 2022, doi: 10.1186/s12880-022-00763-z.
[104] X. Ma, E. C. Ferguson, X. Jiang, S. I. Savitz, and S. Shams, "A multitask deep learning approach for pulmonary embolism detection and identification," *Sci. Rep.*, vol. 12, no. 1, p. 13087, Jul. 2022, doi: 10.1038/s41598-022-16976-9.
[105] P. Ajmera, A. Kharat, J. Seth, S. Rathi, R. Pant, M. Gawali, V. Kulkarni, R. Maramraju, I. Kedia, R. Botchu, and S. Khaladkar, "A deep learning approach for automated diagnosis of pulmonary embolism on computed tomographic pulmonary angiography," *BMC Med. Imag.*, vol. 22, no. 1, p. 195, Nov. 2022, doi: 10.1186/s12880-022-00916-0.
[106] P. A. Grenier, A. Ayobi, S. Quenet, M. Tassy, M. Marx, D. S. Chow, B. D. Weinberg, P. D. Chang, and Y. Chaibi, "Deep learning-based algorithm for automatic detection of pulmonary embolism in chest CT angiograms," *Diagnostics*, vol. 13, no. 7, p. 1324, Apr. 2023, doi: 10.3390/diagnostics13071324.
[107] N. Aydın, Ç. Cihan, Ö. Çelik, A. F. Aslan, A. Odabaş, F. Alataş, and H. Yıldırım, "Segmentation of acute pulmonary embolism in computed tomography pulmonary angiography using the deep learning method," *Tuberk Toraks*, vol. 71, no. 2, pp. 131–137, Jun. 2023, doi: 10.5578/tt.20239916.
[108] F. Condrea, S. Rapaka, L. Itu, P. Sharma, J. Sperl, A. Mohamed Ali, and M. Leordeanu, "Anatomically aware dual-hop learning for pulmonary embolism detection in CT pulmonary angiograms," 2023, *arXiv:2303.17593*, doi: 10.48550/ARXIV.2303.17593.

[109] Y. J. Suh, H. Hong, M. Ohana, F. Bompard, M.-P. Revel, C. Valle, A. Gervaise, J. Poissy, S. Susen, G. Hékimian, M. Artifoni, D. Periard, D. Contou, J. Delaloye, B. Sanchez, C. Fang, G. Garzillo, H. Robbie, and S. H. Yoon, "Pulmonary embolism and deep vein thrombosis in COVID-19: A systematic review and meta-analysis," *Radiology*, vol. 298, no. 2, pp. E70–E80, Feb. 2021, doi: 10.1148/radiol.2020203557.

[110] Y. Sakr, M. Giovini, M. Leone, G. Pizzilli, A. Kortgen, M. Bauer, T. Tonetti, G. Duclos, L. Zieleskiewicz, S. Buschbeck, V. M. Ranieri, and E. Antonucci, "Pulmonary embolism in patients with coronavirus disease-2019 (COVID-19) pneumonia: A narrative review," *Ann. Intensive Care*, vol. 10, no. 1, p. 124, Dec. 2020, doi: 10.1186/s13613-020-00741-0.

JYOTHI CHILLAPALLI received the B.Tech. degree in computer science from Amity University, Mumbai, and the M.Tech. degree in computer science from the Symbiosis Institute of Technology, Pune. She is currently with Philips Healthcare, Bengaluru, as a Software Development Engineer. Her primary field of study has been the development and implementation of novel classification methods for cardiovascular disease.

SHILPA GITE (Member, IEEE) received the Ph.D. degree in deep learning for assistive driving in semi autonomous vehicles from Symbiosis International (Deemed University), Pune, India, in 2019. She is currently an Associate Professor with the AI/ML Department of Symbiosis, Institute of Technology, Pune. She is also an Associate Faculty with the Symbiosis Centre of Applied AI (SCAAI). She has around 15 years of teaching experience. She is guiding Ph.D. students in biomedical imaging, medical image analytics, self-driving cars, and natural language processing areas. She has published more than 70 research articles in international journals and 30 Scopus-indexed international conferences. Her research interests include deep learning, machine learning, medical imaging, and computer vision. She was a recipient of the Best Paper Award from 11th IEMERA Conference held virtually at Imperial College, London, in October 2020.

BUNNY SAINI received the B.Tech. degree (Hons.) in computer science and engineering and in artificial intelligence and machine learning from the Symbiosis Institute of Technology, Symbiosis International (Deemed University), Pune. He is currently associated and working with a prominent financial services firm, in the domain of asset management, where he plays a pivotal role in driving innovation and technological advancements within the industry. He has published studies in the domain of deep learning and reinforcement learning. His research interests include computer vision, deep learning, and natural language processing.

KETAN KOTECHA has expertise and experience of cutting-edge research and projects in AI and deep learning for last more than 25 years. He was an Administrator with Parul University and Nirma University and has several achievements in these roles to his credit. He currently heads the Symbiosis Centre for Applied Artificial Intelligence (SCAAI). He is also a Team Member for the nationwide initiative on AI and deep learning skilling and research named Leadingindia.ai initiative sponsored by the Royal Academy of Engineering, U.K., under Newton Bhabha Fund. He is considered as a foremost expert in AI and aligned technologies. Additionally, with his vast and varied experience in administrative roles, he has pioneered education technology. He has published widely in several excellent peer-reviewed journals on various topics ranging from education policies, teaching-learning practices, and AI for all.

SULTAN ALFARHOOD received the Ph.D. degree in computer science from the University of Arkansas. He is currently an Assistant Professor with the Department of Computer Science, King Saud University (KSU). Since joining KSU in 2007, he has made several contributions to the field of computer science through his research and publications. He has published several research papers on cutting-edge topics, such as machine learning, recommender systems, linked open data, and text mining. His research interests include proposing innovative approaches and techniques to enhance the accuracy and effectiveness of recommender systems and sentiment analysis.